Available online at www.sciencedirect.com
ScienceDirect
Journal of Molecular Graphics and Modelling 26 (2008) 1160–1168
Journal of Molecular Graphics and Modelling
www.elsevier.com/locate/JMGM

Identification of ligand features essential for HDACs inhibitors by pharmacophore modeling

Ya-dong Chen [a], Yong-Jun Jiang [b], Jian-Wei Zhou [b], Qing-Sen Yu [b], Qi-Dong You [a,*]

[a] Department of Medicinal Chemistry, China Pharmaceutical University, 24 Tongjiaxiang, Nanjing 210009, PR China
[b] Ningbo Institute of Technology, Zhejiang University, Ningbo 315104, PR China

Received 1 August 2007; received in revised form 16 October 2007; accepted 16 October 2007
Available online 23 October 2007

Abstract

Histone deacetylases (HDACs) enzyme plays a significant role in transcriptional regulation by modifying the core histones of the nucleosome. It has emerged as an important therapeutic target for the treatment of cancer and other diseases. Inhibitors of HDACs become a new class of anticancer agents and have provoked much interest amongst pharmacologists and cancer researchers. To facilitate the discovery of specific HDACs inhibitors, a 3D chemical-feature-based QSAR pharmacophore model was developed and was well consistent with the structure-functional requirements for the binding of the HDAC inhibitors. Using this model, the interactions between the benzamide MS-275 and HDAC were explored. The result showed that the type and spatial location of chemical features encoded in the pharmacophore are in full agreement with the enzyme-inhibitor interaction pattern identified from molecular docking.

Keywords: Histone deacetylases enzyme; Inhibitor; Pharmacophore model; FlexX; Docking

1. Introduction

Acetylation and deacetylation of chromatin histone protein by histone deacetylase (HDAC) alter chromatin structure and dynamically affect transcriptional regulation. Transcriptionally active genes are associated with highly acetylated core histones, whereas transcriptional repression is associated with low levels of histone acetylation [1–3]. The acetylation status of histones is controlled by the activities of two enzyme families, the histone acetyltransferases (HATs) and histone deacetylases (HDACs) [4,5], both of which are recruited to target genes in complexes with sequence-specific transcription activators. Aberrant regulation of this epigenetic marking system has been shown to cause inappropriate gene expression, a key event in the pathogenesis of various cancers [5–7]. Moreover, evidence demonstrates that inhibition of HDAC triggers growth arrest, differentiation, and/or apoptosis in many types of tumor cells by reactivating the transcription of a small number of genes [8–11]. These findings suggest that modulation of HDAC's function might be targeted for the prevention and/or therapeutic intervention of cancer.

Detailed biochemical studies show that there are three distinctly structural classes of histone deacetylases. Class I and II HDACs are zinc-containing hydrolases. Class III is a series of the NAD-dependent Sir2 family unrelated to the other HDAC classes [12]. Many recent studies have shown that class I/II histone deacetylase enzyme are an emerging therapeutic target for the treatment of cancer and other diseases. Accordingly, in recent years, the development of HDACs inhibitors has been initiated. Till date, several structurally distinct compounds targeting class I/II HDAC enzyme have been reported, and with few exceptions, these can be divided into a few structural classes, including small-molecular hydroxmates, carboxylates, benzamides, electrophilic ketones, and cyclic peptides.

Recently, X-ray crystal structures of human HDAC8 (PDB entry code: 1T64) [13] and histone deacetylase-like protein (HDLP, PDB entry code: 1C3R), a bacterial HDAC homologue, have been resolved and revealed a distinctive mode of protein–ligand interactions [14]. The HDAC catalytic domain consists of a narrow, tube-like pocket spanning the length equivalent to four- to six-carbon straight chains. A Zn^{2+} cation is positioned near the bottom of this enzyme pocket. Accordingly, the wide

* Corresponding author.
E-mail address: qidongyou@gmail.com (Q.-D. You).

1093-3263/$ – see front matter © 2007 Elsevier Inc. All rights reserved.
doi:10.1016/j.jmgm.2007.10.007

variety of structural HDAC inhibitors includes three molecular fragments, namely, a metal-binding domain, which interacts with the active site, a linker domain, which occupies the channel, and a surface recognition domain, which interacts with residues on the rim of the active site. This three-component concept has been proven successful in developing potent HDAC inhibitors [15,16].

Even though a structure-based approach is made possible by knowledge of the structure of the target from crystallography, a ligand-based approach like 3D pharmacophores may provide an alternative and complementary tool for drug design. In order to gain further insight into the structural requirements of HDAC inhibitors, a novel three-dimensional quantitative structure–activity relationship (3D-QSAR) pharmacophore model is developed and further evaluated. This pharmacophore model highlights important binding features of HDAC ligands and may provide guidance for the rational design to discover novel HDAC inhibitors.

2. Materials and methods

2.1. General methodology

All pharmacophore models were generated using the Catalyst 4.10 software (Accelrys Inc., San Diego, CA) on Silicon Graphic O2 workstation. Chemical-feature-based pharmacophore hypotheses can be generated automatically using the HypoGen algorithm within Catalyst, provided that structure–activity relationship data of a well-balanced set of compounds is available.

2.2. Training set and test set selection and conformational models

In automated pharmacophore generation with Catalyst, the selection of the molecules in the training set must follow certain rules: the set must be widely populated (at least 16 items) by structurally diverse representatives covering an activity range of at least four orders of magnitude. The most active compounds should inevitably be included in the training set, and all biologically relevant data should be obtained by homogeneous procedures. Taking into account these requirements, the data sets used in this study were taken from several literatures published by MethyGene Inc. [17–20]. 30 compounds (No. 1–30 in Chart 1) with IC_{50} between 2 and 17 000 nM forming the training set were used to generate HypoGen hypotheses featuring quantitative predictive character. To validate the pharmacophore model, a test set containing 25 HDAC inhibitors of different activity classes was analyzed (No. 31–55 in Chart 2). All molecules were built using the 2D and 3D sketcher of Catalyst. A conformational set was generated for each molecule using the poling algorithm and the ''best-quality conformational analysis'' method, based on CHARMm force field. All other parameters used were kept at their default settings. A maximum of 250 conformations within 20 kcal/mol in energy from the global minimum were saved. The molecules associated with their conformational models were then submitted to catalyst hypothesis generation.

2.3. Generation of pharmacophore hypotheses with HypoGen

The algorithm HypoGen implemented in the Catalyst package was used to derive automated SAR pharmacophore models. It has been suggested that the hydroxmate derivatives act by coordinating the zinc ions required for HDAC activity. In the pharmacophore-based investigation of HDAC inhibitors involving catalyst, on the basis of the chemical features of compounds in the training set and the proposed mechanism of action, the following chemical functions were selected in the feature dictionary: hydrogen bond acceptor (HBA), hydrogen bond donor (HBD), hydrophobic (HY), hydrophobic aliphatic (HYAl), and hydrophobic aromatic (HYAr) groups. In fact, even if the metal-binding function is not included in the catalyst feature dictionary, it can be replaced by a standard hydrogen bond acceptor/donor function [21]. The uncertain factor for each compound represents the ratio range of uncertainty in the activity value based on the expected statistical straggling of biological data collection. In our case, an uncertainty of 2.0 was preferred over the default factor of 3.0. The chosen value of 2.0 is more convenient for HDAC inhibitors because their activities barely span the required four orders of magnitude; this choice has been further confirmed by preliminary calculations and by other literature evidence [22]. Pharmacophores were then computed using HypoGen module and the top 10 scoring hypotheses were exported.

2.4. Molecular docking

Docking of the compound MS-275 into the binding pocket of HDLP was carried out using the FlexX [23] program available within SYBYL6.9 package. FlexX employs a fast algorithm for the flexible docking of small ligands into a fixed protein binding site using an incremental construction process. Standard parameters of the FlexX program as implemented in SYBYL6.9 were used during docking.

3. Result and discussion

3.1. Pharmacophore modeling

A powerful approach in virtual drug design is the automated generation of pharmacophore models within the catalyst software package [24], as a large number of successful applications in medicinal chemistry have been clearly demonstrated [25–27].

Catalyst produced 10 hypotheses. The top-ranked one, Outhypo-11714.1 (Hypo1 for simplicity), consists of one hydrogen bond acceptor, one hydrogen donor, and three hydrophobic features. Hypo1 is the best pharmacophore hypothesis resulting from this study, as it is characterized by the highest cost difference, lower errors, lowest root mean square (rms) divergence, and best correlation coefficient (Table 1). The quality of the generated pharmacophore

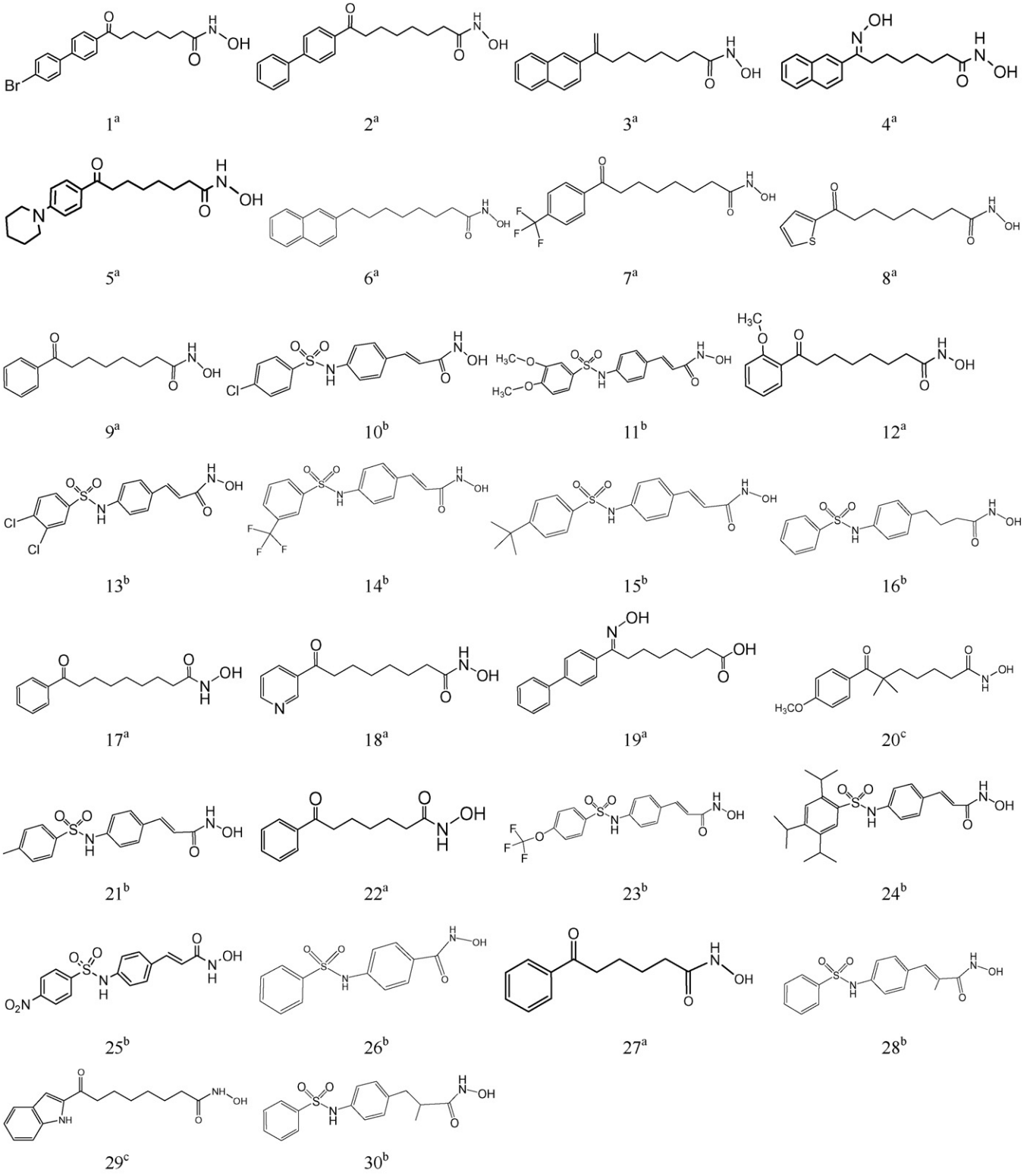

Chart 1. 2D Chemical structures of the 30 molecules forming the training set used to obtain HypoGen pharmacophore hypotheses. (a) Ref. [17], (b) Ref. [18], (c) Ref. [19].

hypotheses was evaluated by considering the cost functions calculation by HypoGen module during hypotheses generation. In detail, the null cost of the 10 top-scored hypotheses was equal to 213.004, the fixed cost value was 104.789, and the configuration cost was 16.572. As the total cost of Hypo1 was equal to 123.259, the large difference between null and total hypothesis cost, Δcost = 89.745, coupled with a high correlation coefficient, $r = 0.924$, and a reasonable root mean square deviation, rms = 1.109. The values indicated a great predictability of the 3D-QSAR pharmacophore and confirmed that it

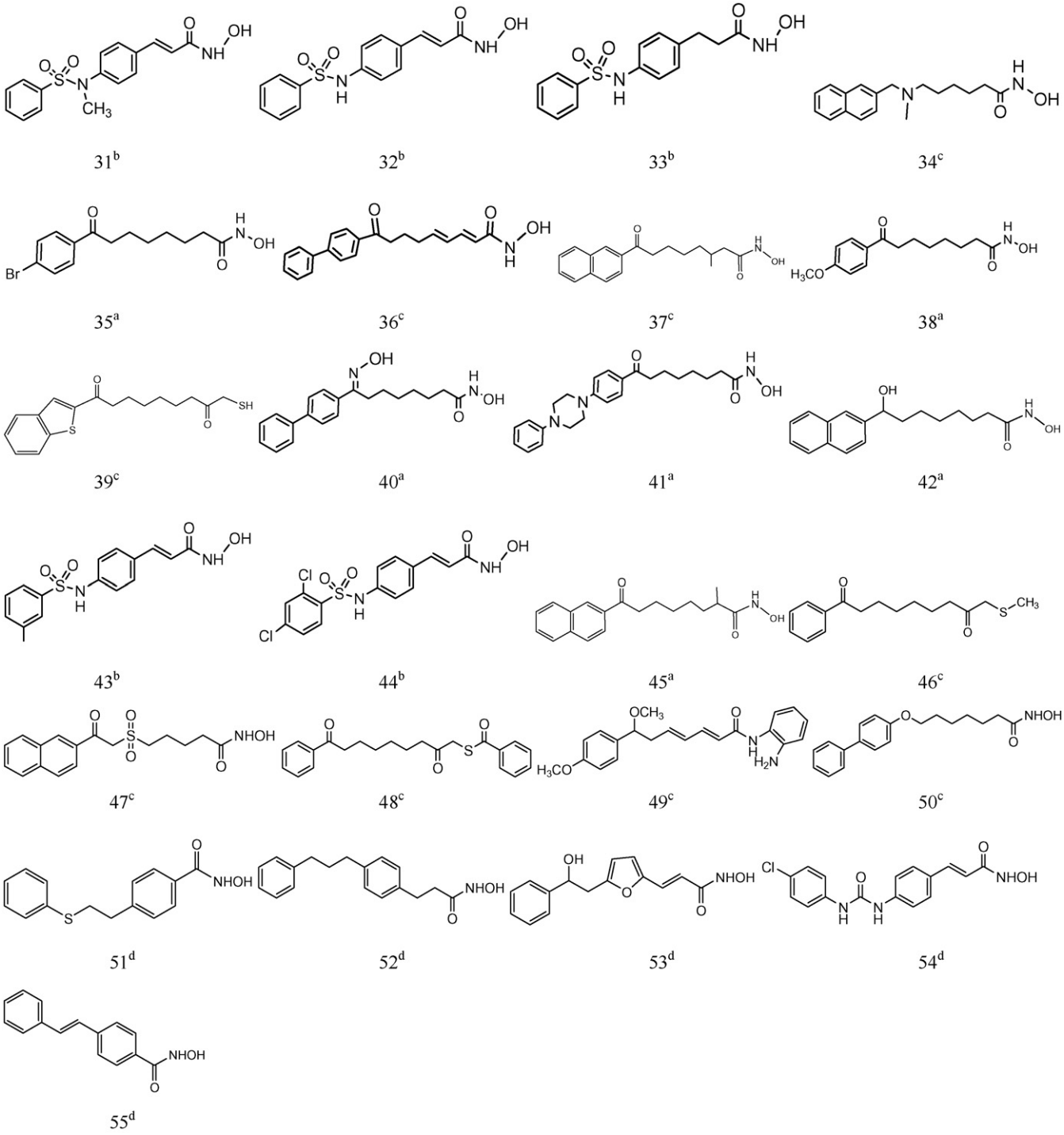

Chart 2. 2D Chemical structures of the 25 molecules forming the test set. (a) Ref. [17], (b) Ref. [18], (c) Ref. [19], (d) Ref. [20].

did not come about by chance; Hypo1 was thus retained for further analysis.

Besides this cost analysis, the most obvious method to validate Hypo1 is to check for its capacity to correctly predict the activity of the training set compounds. Table 2 lists the Hypo1 estimated activity values, together with the corresponding errors (the ratio between calculated and experimental activity). As you can see from this table, most of the IC_{50} values were predicted correctly.

Fig. 1a depicts one of the most active conformations of compound 1 in the training set mapped onto Hypo1. As you can see from this figure, compound 1 fits all features of the pharmacophore model Hypo1 very well. The aliphatic chain (seven-methylene linker) and two phenyl rings of the molecule overlap with the three hydrophobic features of Hypo1, respectively. The oxygen atom of the CO group of the hydroxamic acid serves as a hydrogen bond acceptor (HBA). The hydrogen donor point is located on the oxygen atom of the

Table 1
Results of pharmacophore hypotheses generated by catalyst/HypoGen

Hypo[a]	Total cost	Cost diff.[b]	rms deviation	Correlation (r)	Features
Hypo1	123.259	89.745	1.109	0.924	HBA, HBD, HY, HY, HY
Hypo2	131.006	81.998	1.313	0.892	HBA, HBD, HY, HY, HY
Hypo3	134.756	78.248	1.412	0.873	HBA, HBD, HY, HY, HY
Hypo4	136.574	76.43	1.450	0.866	HBA, HBA, HY, HY, HY
Hypo5	138.325	74.679	1.482	0.859	HBA, HBA, HY, HY, HY
Hypo6	138.821	74.183	1.498	0.856	HBA, HBA, HY, HY, HY
HYpo7	141.81	71.194	1.546	0.846	HBA, HBA, HY, HY, HY
Hypo8	142.695	70.309	1.557	0.843	HBA, HBD, HY, HY, HY
Hypo9	144.886	68.118	1.621	0.829	HBA, HBD, HY, HY
Hypo10	145.395	67.609	1.636	0.825	HBA, HBD, HY, HY

[a] Number for the hypothesis are consistent with the numeration as obtained by the hypothesis generation.
[b] Cost difference between the null cost and the total cost, the null cost of the 10 top-scored hypotheses is 213.004, the fixed cost value is 104.789, and the configuration cost is equal to 16.572.

OH group of the hydroxamic acid. Thus, the most active compound 1 in the training set maps closely with the statistically most significant hypothesis, and the predicted activity of 1 toward Hypo1 is reasonable. Fig. 1b also shows, as an example, the mapping on Hypo1 of the training set compound 30, for which the two oxygen atoms of hydroxamic (CONHOH) acid moiety serve as HBA and HBD features, respectively. The two hydrophobic features overlap with the phenyl rings present in the molecule, whereas the third hydrophobic feature mapping is missing.

Table 2
Actual and estimate activity of the training set molecular based on the pharmacophore model Hypo1

Compd. no.	Fit	IC_{50} [nM]		Errors[a]
		Estimate	Actual	
1	8.75	2.3	2	1.1
2	8.47	4.3	5	−1.2
3	8.1	10	8	1.3
4	7.85	18	8.5	2.1
5	7.73	23	9.5	2.5
6	7.75	22	25	−1.1
7	7.32	61	45	1.4
8	7.33	60	50	1.2
9	7.2	81	65	1.2
10	6.81	200	75	2.6
11	7.26	70	90	−1.3
12	7.33	59	95	−1.6
13	7.29	66	100	−1.5
14	7.43	47	100	−2.1
15	7.12	96	100	−1
16	6.72	240	100	2.4
17	6.96	140	140	−1
18	7.36	56	150	−2.7
19	6.78	210	200	1
20	6.52	350	250	1.4
21	6.71	250	300	−1.2
22	5.68	2700	500	5.3
23	6.55	360	600	−1.7
24	6.68	270	600	−2.2
25	5.64	2900	700	4.2
26	6.3	630	900	−1.4
27	5.68	2700	1500	1.8
28	6.06	1100	2000	−1.8
29	5.69	2600	4000	−1.5
30	5.87	1700	17000	−9.8

[a] Value in the error column represents the ratio of the estimated activity to the tested activity or its negative inverse if the ratio is less than one.

Finally, we used Hypo1 to analyze a test set containing 25 compounds of different activity classes to check the predictive power of this pharmacophore hypothesis. Structure data of test set compounds are shown in Chart 2. Most of members of test set were correctly predicted, and the result was reported in Table 3. We also used Hypo1 to perform a regression analysis with the test set compounds in order to check the predictive power of this model. Linear regression of the predicted activities for testing set inhibitors versus the experimental ones gave a fairly good correlation coefficient of 0.896 (see Fig. 2), confirming the validity of the most statistically significant HypoGen hypothesis in predicting the HDAC inhibitory activity.

3.2. Evaluating the fit of the pharmacophore to the binding site of the crystal structure of HDLP

In an attempt to evaluate the fit of the pharmacophore to the binding site of crystal structure of HDLP, the pharmacophore model Hypo1 was compared to the bound conformation of the compound TSA in complex with HDLP. The bound conformation of the compound TSA, which was extracted from crystal structure of HDLP (pdb entry code: 1c3r), was mapped onto the pharmacophore model Hypo1 using the ''best fit '' option, and superimposed to the Catalyst conformation from 3D mapping onto the pharmacophore model Hypo1 (see Fig. 3a). The root mean square distance (RMS) between the heavy atom positions of the bound and the Catalyst conformation was 1.19 Å. For the compound TSA, both conformations are quite well overlaid as shown in Fig. 3a. The bound conformation of the compound TSA is able to successfully fit all chemical features in the Hypo1 model.

To further assess the pharmacophore Hypo1, we compare the pharmacophore model with the active site of HDLP crystal structure. A summary of the mappings of the pharmacophore Hypo1 to the HDLP crystal structure is shown in Fig. 3b. The pharmacophore Hypo1 is in good agreement with the target-based pharmacophore. The Catalyst model appears to accommodate into a narrow tubular pocket of the active site.

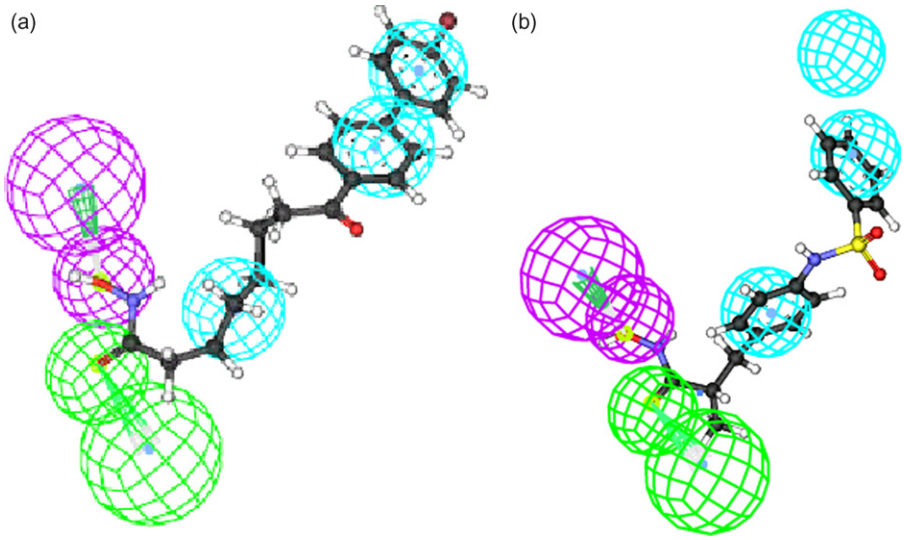

Fig. 1. Training set compound 1 (a) and compound 30 (b) mapped to Hypo1. Hypothesis features are color-coded as follows: hydrophobic aromatic, light blue; hydrogen bond donor, violet; hydrogen bond acceptor, green.

In the pharmacophore Hypo1, the HBA and HBD features (mapped on the CO and OH groups of the hydroxamic acid moiety) correspond to the metal-binding function and represent that they coordinate with Zn^{2+} cation. This is a common interaction between HDAC and inhibitor. In addition, the hydrophobic/π–π stacking interactions between ligand and HDAC enzyme may equally play a crucial role because the other three of five pharmacophore features are hydrophobic features. One of the three hydrophobic features, HY1, which mapped to an aliphatic or aromatic chain as linker of HDAC inhibitors, locates at the hydrophobic region inside the tube-like pocket which is surrounded by Phe198 and Phe141 residues of the active site. HY1 is responsible for interacting with the two juxtaposed phenyl moieties of Phe-141 and Phe-198. The other two hydrophobic features (HY2 and HY3) mapped to the cap group of HDAC inhibitors which make contacts at the pocket entrance. Interestingly, this finding indicates that the two hydrophobic features make HDAC inhibitors with larger

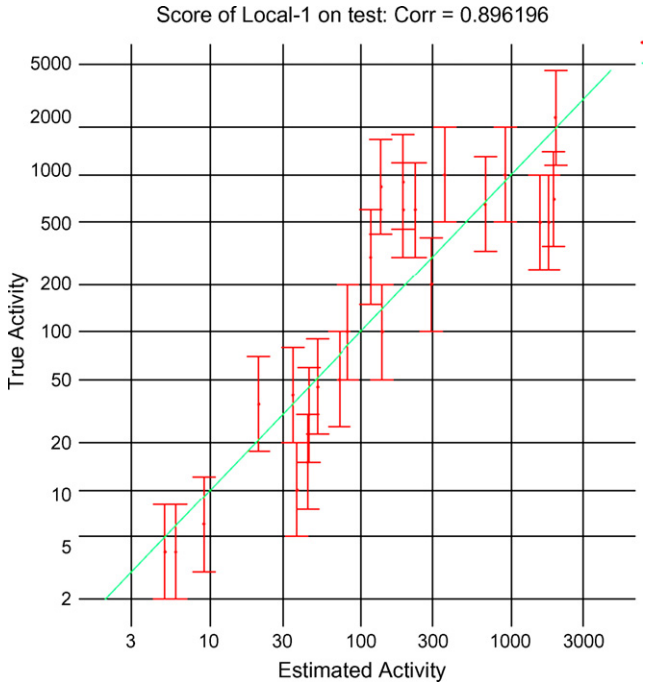

Fig. 2. Correlation line displaying the observed vs. estimated IC_{50} values (nM) of the test set by using the pharmacophore model Hypo1 (*Y*-axis shows the experimental activity, and *X*-axis represents the estimated activity).

Table 3
Actual and estimate activity of the test set molecular based on the pharmacophore model Hypo1

Compd.	IC_{50} (nM)		Errors[a]
	Actual	Estimate	
31	600	230	−2.6
32	200	360	1.8
33	100	92	−1.1
34	50	80	1.6
35	45	56	1.3
36	40	38	−1.1
37	30	49	1.6
38	15	48	3.2
39	10	40	3.3
40	4	5.0	4.0
41	6	9	1.5
42	35	22	−1.6
43	100	160	1.6
44	300	130	−2.2
45	600	280	−2.2
46	500	2400	4.7
47	1000	1200	1.2
48	700	2600	3.6
49	1000	440	−2.3
50	4	4.8	1.2
51	900	230	−4.0
52	650	850	1.3
53	500	2000	4.1
54	840	160	−5.3
55	2300	2600	1.1

[a] Value in the error column represents the ratio of the estimated activity to the tested activity or its negative inverse if the ratio is less than one.

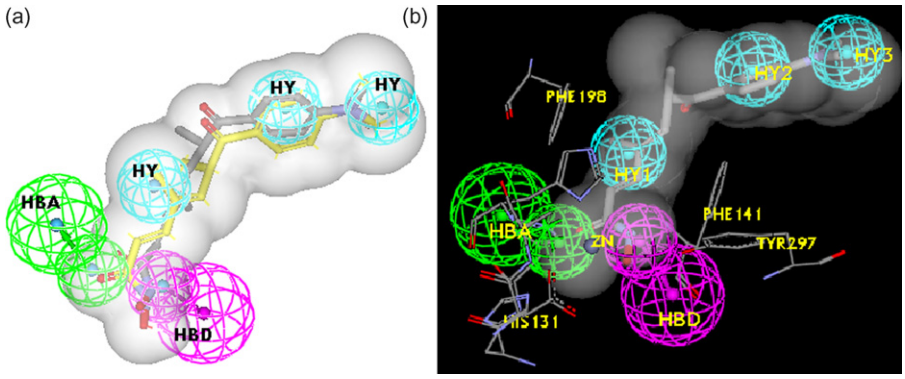

Fig. 3. (a) The catalyst conformation from 3D mapping of TSA onto pharmacophore Hypo1, the bound conformation from X-ray crystal structure and integrated shape are presented. The catalyst confirmation in grey, bound conformation in yellow (HBA, hydrogen bond acceptor; HBD, HBA, hydrogen bond donor; HY, hydrophobic region). (b) The pharmacophore Hypo1 mapped to a HDLP crystal structure. The hydrogen bond acceptor feature is shown in green. The hydrogen donor feature is shown in purple. The hydrophobic features are shown in light blue. The carbon atoms of the HDLP residues that are shown in grey. Zinc ion is shown in sphere. The ligand TSA is shown in stick. The shaded part that surrounds the molecule shows the shape.

surface contact areas at the pocket entrance to facilitate the hydrophobic interaction with surface of no specific residues. Overall, these observations confirm that the proposed ligand-based pharmacophore model can fit the binding pocket and matches well with the topology of the active site. The pharmacophore model derived from ligands is in good agreement with the structural information derived X-ray structure of the binding domain of HDLP and supports the target-based one deduced from the X-ray crystal structure.

3.3. Explanation of key interactions between MS-275 and HDLP by pharmacophore model Hypo1 together with docking

Though the pharmacophore model was derived from hydroxamic acid derivatives, chemical features in the Hypo1 also appear to be shared by a wide range of HDAC inhibitors. The benzamide derivative Ms-275, which is currently in phase II clinical trials, was discovered to have HDAC inhibitory activity in low micromolar range [28]. The exact nature of the benzamide moiety interaction with the active site of the enzyme has not been fully elucidated. Here, MS-275 was mapped onto pharmacophore model Hypo1 in Catalyst using the ''best fit'' option to analyze the key groups interacting with the residues of the active site. The predicted HDAC1 inhibitory activity of MS-275 (IC_{50}) is 181 nM, which compared well with the actual value of 185 nM [13]. The mapping on Hypo1 is shown in Fig. 4a. As we can see from this figure, MS-275 fits four of the five features and misses one of three hydrophobic features (HY3). Two hydrophobic interactions are mapped by phenyl rings of the molecule, respectively. The amino substitute of the benzamide serves as a hydrogen bond donor (HBD). Another

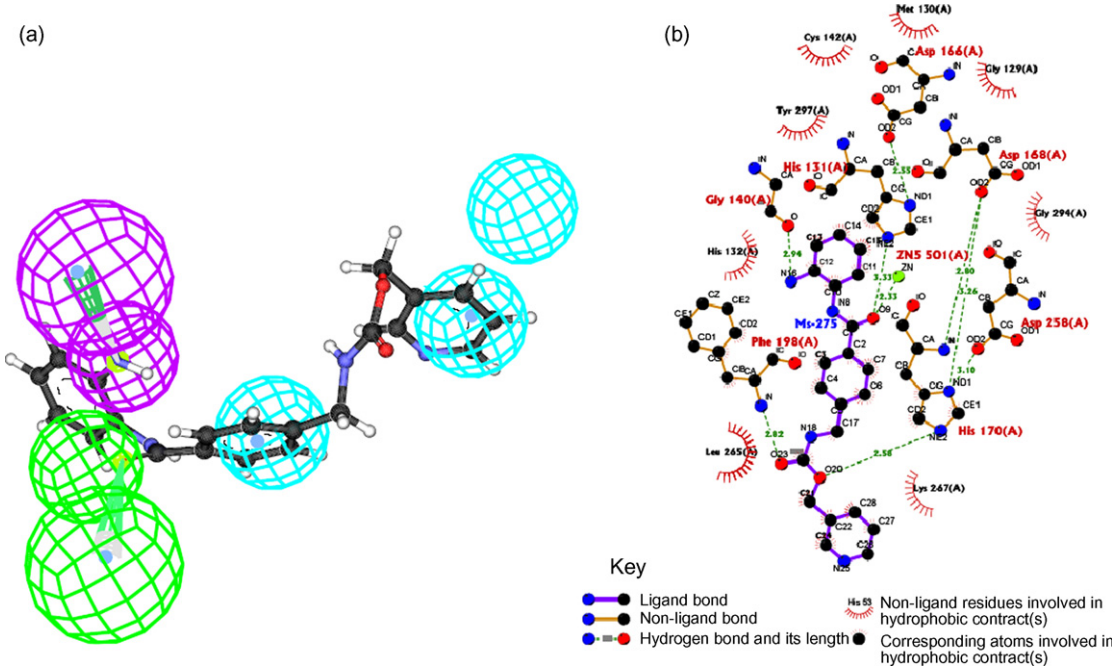

Fig. 4. (a) Compound Ms-275 mapped to Hypo1. Hypothesis features are color-coded as follows: hydrophobic aromatic, light blue; hydrogen bond donor, violet; hydrogen bond acceptor, green. (b) The docking result is analyzed using the ligplot4.22 to identify some specific contacts between atoms of Ms-275 and HDLP.

hydrogen bond acceptor (HBA) is located on the carbonyl oxygen atom of the amide group.

To validate the possible binding model derived from pharmacophore model Hypo1, FlexX, molecular docking program, was employed to gain insight into the binding mode between MS-275 and the active site of HDLP. First, the crystal structure of bacterial HDLP complexed with TSA was performed by FlexX. A superposition of FlexX-docked TSA onto the crystallographic geometry yielded a root mean square (rms) deviation of 0.92 Å and revealed that FlexX performed well in reproducing the binding conformation of TSA (result not shown). Then, the compound MS-275 was docked into the active site of HDLP. Fig. 4b reports the main interactions between Ms-275 and HDLP. A marked similarity was observed between features proposed by the pharmacophore models and ligand binding features in the docked structure. The carbonyl oxygen atom of the amide group is coordinated to the zinc ion, which is critical for the HDAC catalysis, and forms one hydrogen bond with His131. The amino substituent of the benzamide interacts with Gly140 by a hydrogen bond. The phenyl ring in the middle of the molecule has a hydrophobic interaction with the channel of the active site surrounded by Phe198, His170, Leu265. The pyridine ring interacts with the residues at the entrance of the active site (such as Lys267, etc.) by hydrophobic interaction. We have compared the pharmacophore mapping of Ms-275 with corresponding enzyme–ligand complex obtained from molecular model. Our docking result is in perfect agreement with the hypothesis. It is interesting to note that all key interactions between Ms-275 and HDLP are all encoded in the pharmacophore though Ms-275 is structurally different from hydroxamic acid. In conclusion, the chemical features that a molecule should possess in order to be a good HDAC enzyme inhibitor are all represented in our pharmacophore, although it has been generated using a ligand-based approach and without considering structural information of the target.

4. Conclusions

In this work, we have built quantitative pharmacophore models from a training set of 30 hydroxamic acid compounds active as inhibitors of the HDAC1 enzyme. The best pharmacophore consists of five pharmacophore features, including a hydrogen bond donor, a hydrogen bond acceptor, three hydrophobic features, having a correlation coefficient of 0.924. Besides, this hypothesis is further validated by an external test of 25 compounds. The pharmacophore showed distinct chemical features that may be responsible for the activity of the inhibitors. The type and spatial location of the chemical feature agree perfectly with the pattern of enzyme-inhibitor interactions identified from crystallography. Therefore, the pharmacophore completely fulfills the requirements for an effective interaction of the inhibitors with the active site of HDAC. The knowledge concerning the pharmacophore which reflects structural requirements for interaction with the target is expected to be useful in identifying and designing inhibitors with greater selectivity toward HDAC1. We intend to utilize the information to undertake 3D searches on large databases of drug-like molecules to identify a new generation of HDAC1 inhibitors.

References

[1] M.J. Pazin, J.T. Kadonaga, What's up and down with histone deacetylation and transcription? Cell 89 (3) (1997) 325–328.

[2] P.A. Wade, D. Pruss, A.P. Wolffe, Histone acetylation: chromatin in action, Trends Biochem. Sci. 22 (4) (1997) 128–132.

[3] A.P. Wolffe, Transcriptional control Sinful repression, Nature 387 (1997) 16–17.

[4] K. Struhl, Histone acetylation and transcriptional regulatory mechanisms, Genes Dev. 12 (1998) 599–606.

[5] T. Kouzarides, Histone acetylases and deacetylases in cell proliferation, Curr. Opin. Genet. Dev. 9 (1999) 40–48.

[6] P.A. Wade, Transcriptional control at regulatory checkpoints by histone deacetylases: molecular connections between cancer and chromatin, Hum. Mol. Genet. 10 (2001) 693–698.

[7] W.D. Cress, E. Seto, Histone deacetylases, transcriptional control, and cancer, J. Cell Physiol. 184 (2000) 1–16.

[8] P. Marks, R.A. Rifkind, V.M. Richon, R. Breslow, T. Miller, et al., Histone deacetylases and cancer: causes and therapies, Nat. Rev. Cancer 1 (2001) 194–202.

[9] M. Jung, Inhibitors of histone deacetylase as new anticancer agents, Curr. Med. Chem. 8 (2001) 1505–1511.

[10] C.M. Grozinger, S.L. Schreiber, Deacetylase enzymes: biological functions and the use of small-molecule inhibitors, Chem. Biol. 9 (2002) 3–16.

[11] R.W. Johnstone, Histone-deacetylase inhibitors: novel drugs for the treatment of cancer, Nat. Rev. Drug Discov. 1 (2002) 287–299.

[12] G. Blander, L. Guarente, The Sir2 family of protein deacetylases, Annu. Rev. Biochem. 73 (2004) 417–435.

[13] A. Vannini, C. Volpari, G. Filocamo, E.C. Casavola, M. Brunetti, D. Renzoni, P. Chakravarty, C. Paolini, R.D. Francesco, P. Gallinari, C. Steinkuhler, S.D. Marco, Crystal structure of a eukaryotic zinc-dependent histone deacetylase, human HDAC8, complexed with a hydroxamic acid inhibitor, Proc. Natl. Acad. Sci. U.S.A. 101 (42) (2004) 15064–15069.

[14] M.S. Finnin, J.R. Donigian, A. Cohen, V.M. Richon, R.A. Rifkind, et al., Structures of a histone deacetylase homologue bound to the TSA and SAHA inhibitors, Nature 401 (1999) 188–193.

[15] M. Jung, G. Brosch, D. Kolle, H. Scherf, C. Gerhauser, et al., Amide analogues of trichostatin A as inhibitors of histone deacetylase and inducers of terminal cell differentiation, J. Med. Chem. 42 (1999) 4669–4679.

[16] S.M. Sternson, J.C. Wong, C.M. Grozinger, S.L. Schreiber, Synthesis of 7200 small molecules based on a substructural analysis of the histone deacetylase inhibitors trichostatin and trapoxin, Org. Lett. 3 (2001) 4239–4242.

[17] S.H. Woo, S. Frechette, E.A. Khalil, G. Bouchain, A. Vaisburg, N. Bernstein, O. Moradei, S. Leit, M. Allan, M. Fournel, M.-C. Trachy-Bourget, Z. Li, J. Besterman, D. Delorme, Structurally simple trichostatin A-like straight chain hydroxamates as potent histone deacetylase inhibitors, J. Med. Chem. 45 (2002) 2877–2885.

[18] R. Lavoie, G. Bouchain, S. Frechette, S.H. Woo, E.A. Khalil, S. Leit, M. Fournel, P.T. Yan, M.-C. Trachy-Bourget, C. Beaulieu, Z.M. Li, J. Besterman, D. Delorme, Design and synthesis of a novel class of histone deacetylase inhibitors, Bioorg. Med. Chem. Lett. 11 (2001) 2847–2850.

[19] Delorme, Daniel, Woo, Soon, Hyung, Vaisburg, Arkadii, Inhibitors of Histone Deacetylase, Methylgene, Inc. Int. Patent Appl. WO 01/70675, 2001.

[20] Delorme, Daniel, Ruel, Rejean, Lavoie, Rico, Thibault, Carl, Abou-Khalil, Elie. Inhibitors of Histone Deacetylase, Methylgene, Inc. Int. Patent Appl. WO 01/38322, 2001.

[21] H. Li, J. Sutter, R. Hoffman, HypoGen: an automated system for generating 3D predictive pharmacophore models, in: Pharmacophore

Perception, Development, and Use in Drug Design, International University, La Jolla, CA, 2000, pp. 171–189.
[22] F. Briens, R. Bureau, S. Rault, Applicability of catalyst in ecotoxicology, a new promising tool for 3D-QSAR: study of chlorophenols, Ecotoxicol. Environ. Saf. 43 (1999) 241–251.
[23] M. Rarey, B. Kramer, T. Lengauer, G. Klebe, A fast flexible Docking method using an incremental construction algorithm, J. Mol. Biol. 261 (1996) 470–489.
[24] Catalyst, version 4.10 (software package); accelrys, Inc., San Diego, 2004.
[25] M.L. Barreca, S. Ferro, A. Rao, L. De Luca, M. Zappala, A.M. Monforte, Z. Debyser, M. Witvrouw, A. Chimirri, Pharmacophore-based design of HIV-1 integrase strand-transfer inhibitors, J. Med. Chem. 48 (2005) 7084–7088.
[26] A. Palomer, F. Cabre, J. Pascual, J. Campos, M.A. Trujillo, A. Entrena, M.A. Gallo, L. Garcia, D. Mauleon, A. Espinosa, Identification of novel cyclooxygenase-2 selective inhibitors using pharmacophore models, J. Med. Chem. 45 (2002) 1402–1411.
[27] R. Di Santo, M. Fermeglia, M. Ferrone, M.S. Paneni, R. Costi, M. Artico, A. Roux, M. Gabriele, K.D. Tardif, A. Siddiqui, S. Pricl, Simple but highly effective three-dimensional chemical-feature-based pharmacophore model for diketo acid derivatives as hepatitis C virus RNA-dependent RNA polymerase inhibitors, J. Med. Chem. 48 (2005) 6304–6314.
[28] T. Suzuki, T. Ando, K. Tsuchiya, N. Fukazawa, A. Saito, Y. Mariko, T. Yamashita, O. Nakanishi, Synthesis and histone deacetylase inhibitory activity of new benzamide derivatives, J. Med. Chem. 42 (15) (1999) 3001–3003.